

Ionic solids at elevated temperatures and/or high pressures: lattice dynamics, molecular dynamics, Monte Carlo and *ab initio* studies

Neil L. Allan,^a Gustavo D. Barrera,^b John A. Purton,^c Chris E. Sims^a and Mark B. Taylor^a

^a School of Chemistry, University of Bristol, Cantock's Close, Bristol UK BS8 1TS

^b Departamento de Química, Universidad Nacional de la Patagonia SJB, Ciudad Universitaria, (9000) Comodoro Rivadavia, Argentina

^c CLRC, Daresbury Laboratory, Warrington, Cheshire UK WA4 4AD

Received 29th October 1999, Accepted 20th January 2000

We show how quasiharmonic lattice dynamics, Monte Carlo, molecular dynamics and *ab initio* techniques are increasingly able to provide valuable information concerning the behaviour of perfect and disordered polar solids over a broad range of temperatures and pressures. A wide range of examples includes (i) the thermodynamics of the pressure-induced phase transformation in MgF₂ between the rutile and fluorite structures, (ii) the negative thermal expansion of ZrW₂O₈, (iii) surface and defect free energies as a function of temperature, (iv) solid solutions of oxides and silicates, (v) possible mechanisms for the B1–B2 phase transition in SrO, and (vi) MnO and NiO at high pressure. Particular attention is paid to the merits and limitations of the various methodologies and the advantages of using a combination of these techniques to obtain a broader understanding of particular problems.

Introduction

The continuing growth in computer power has led to a tremendous increase in the importance of computer simulation to the understanding and design of complex materials and minerals.¹ In particular the behaviour of solids at elevated temperatures and/or high pressure is a key aspect of condensed matter chemical physics in areas as diverse as the modelling of explosives, ceramics processing and geophysics. Computational techniques offer a particularly attractive approach in many of these fields, especially where experimental data are sparse and difficult to obtain. For example, phase changes and the associated changes in thermodynamic properties (*e.g.*, expansivity and compressibility) can be particularly important in geochemistry but often remain far from straightforward to investigate experimentally.

Theoretical studies of solids have most commonly involved first principles (*ab initio*) electronic structure calculations, classical molecular dynamics (MD) and Monte Carlo (MC) simulations, or energy minimisation in the static limit ($T = 0$ in the absence of lattice vibrations). Somewhat less attention has been paid to lattice dynamics in which phonon frequencies are calculated directly. Historically, most often each particular technique has been used in isolation. It is important to distinguish *ab initio* methods (here periodic Hartree–Fock (HF) and density-functional theory (DFT)) and *simulation* methods (here MD, MC, quasiharmonic lattice dynamics and energy minimisation) which use interatomic potentials to describe the interactions between the ions. These interatomic potentials are increasingly derived from *ab initio* calculations, rather than fitted empirically. The modelling of complex solids such as crystals with large unit cells, crystals with defects, solid solutions and surfaces presents severe computational demands if high precision is required and all these techniques have their own merits and limitations. Computational resources presently available normally restrict the use of *ab initio* first principles calculations, which are in principle the most accurate and generally applicable, to systems with relatively small unit cells. In

particular the calculation of thermal effects *via ab initio* methods is sufficiently computationally demanding that much work concerned with properties at finite temperature (MC, MD or lattice dynamics) uses potential-based approaches.

Molecular dynamics and classical Monte Carlo rely on generating a set of system states representative of the equilibrium configuration and averaging over this set; as the average is taken over more states the accuracy of calculated properties improves. Molecular dynamics calculations explicitly include time as a variable and so make it possible to examine related properties such as ion diffusion. We show below how a novel hybrid MC approach combining both MC and MD steps can be particularly valuable for overcoming kinetic barriers in disordered solids and sampling a large number of different configurations.

Lattice dynamics is a relatively inexpensive technique, which avoids the kinetic barriers and critical slowing-down effects suffered by MC and MD, and in general does not rely on long runs for high precision. Surprisingly, it has been somewhat neglected in recent years. The bulk of the computational effort is usually expended in the optimisation problem involving the determination of the equilibrium geometry of the crystal. After this direct calculation of the required properties such as entropy and heat capacity is generally rapid. Several examples later include a comparison of the results of MD and/or MC studies with those from quasiharmonic lattice dynamics. Quasiharmonic lattice dynamics is particularly useful at temperatures below the Debye temperature where classical MC and MD simulations fail due to their neglect of quantum effects. Lattice dynamics also provides an extremely sensitive test for interatomic potentials, in that the presence of imaginary frequencies may immediately indicate a given potential set is invalid in a way that would be far from straightforward for MC and MD. An important additional advantage over MC and MD is that free energies can be calculated directly to high accuracy and we shall see how this provides an efficient route to the free energy of particular configurations of disordered solids and hence, for example, to the

excess functions of non-ideal solid solutions. A disadvantage is the failure of the quasiharmonic approximation at high temperatures as the melting point is approached.

In this paper we concentrate on a set of illustrative examples. We start with a brief discussion of the various theoretical methods, with some emphasis on lattice dynamics. Our account is by no means intended to be comprehensive since excellent reviews of these techniques are available elsewhere.^{2–4} A major aim of this paper is to show that, in many case studies, a broader understanding of the problem of interest is best achieved by the combination of *several* of these powerful techniques (*cf.* ref. 5). Our first example is the behaviour of MgF₂ at high temperatures and high pressures, using interionic potentials obtained from HF calculations. Further case studies include simulations of ceramics with negative thermal expansion, and the calculation of the temperature dependence of surface and defect free energies, based on a full minimisation of all atomic coordinates. Simulations have previously been largely restricted to the study of end-member compounds, excluding many industrially important ceramics and naturally occurring minerals and so our next examples are solid solutions of oxides and silicates. These systems (MgO/MnO, MgO/CaO and MgSiO₃/MnSiO₃) show how novel simulation techniques recently proposed by us can be used to investigate the influence of *high* impurity or defect concentrations on thermodynamic properties and phase transitions. Also presented are results relating to the mechanisms of solid-state phase transitions as well as the thermodynamics. Finally we turn to transition metal oxides (MnO and NiO) at high pressures, and investigate possible phase changes and structural distortions, using first principles calculations. We make predictions and suggest possible experiments where there is disagreement between the conclusions from different theoretical approaches.

Theoretical methods

Ab initio calculations

In this paper we report the results of self-consistent field (SCF) linear-combination-of-atomic-orbitals periodic HF or DFT calculations as implemented in the CRYSTAL computer code developed by the Daresbury and Turin groups. This code has been described in detail previously.^{2,6} These all-electron calculations all use extended Gaussian basis sets comprised of localized crystal orbitals appropriate for the solid state. The numerical values of the tolerance parameters involved in the evaluation of the infinite Coulomb and exchange series were identical to those in previous work^{7,8} and chosen, as before, to ensure high numerical accuracy. The reciprocal space integration utilized the Monkhorst–Pack sampling scheme⁹ with a shrinking factor of 8 and an SCF convergence criterion based on differences in the energy of the unit cell of less than 10^{–4} mHa. In one case, SrO, we have used the Hay and Wadt small core pseudopotential,¹⁰ as in previous work.¹¹ SCF DFT calculations were based on the Dirac–Slater–LSD exchange potential and the Vosko–Wilk–Nusair parameterization of the Ceperley–Alder free electron gas correlation contribution.¹² In one example, the magnitude of *a posteriori* correlation corrections¹³ to the HF energy based on the correlation-only density functional of Perdew¹⁴ has been examined. All electronic structure calculations are in the static limit. The results are used to extract accurate interatomic potentials for subsequent use in MC, MD and lattice dynamics simulations, and, more directly, to compute the equation of state in the static limit and to investigate possible high-pressure phase transitions.

Lattice dynamics

We have recently developed new code¹⁵ based on quasiharmonic lattice dynamics (QLD) and lattice statics designed

for the efficient study of solids and slabs with periodic structures and *many* internal strains. QLD, in principle, gives high precision, and in many applications has been shown to be a valid approximation up to two-thirds of the melting temperatures.¹⁶ For Li₂O, it has also been demonstrated previously that for properties such as the thermal expansion there is good agreement up to about two-thirds of the melting point between QLD and MD calculations based on identical interionic potentials.⁵

To perform the structure optimisation (free energy minimisation) it is necessary to obtain derivatives of the free energy with respect to the geometrical coordinates. Previous approaches to this problem¹⁷ have used the zero static internal stress approximation (ZSISA), or minor variations thereof, in which only the external coordinates (dimensions of the unit cell) are relaxed using fully dynamic free energy derivatives, while the internal coordinates (positions of the ions within the unit cell) are relaxed using static energy derivatives. This approach is popular since static energy derivatives are easy to calculate analytically, and quite rapidly, while only a small number of free energy derivatives are required, and these are obtained numerically. Even for moderately sized unit cells numerical differentiation of the free energy with respect to all internal coordinates is normally prohibitively expensive. Our new code calculates the full set of free energy first derivatives analytically (as described below) and for the first time a full minimisation of the quasiharmonic free energy with respect to all internal and external variables for large unit cells is possible. As demonstrated previously¹⁸ ZSISA gives the external variables correctly to first order, but the internal coordinates will be estimated incorrectly. Our code presently uses two-body and three-body potentials to represent the non-Coulombic interactions between the ions. Polarizability effects may be readily incorporated by using the well-known Dick–Overhauser shell model,¹⁹ in which each ion consists of a massless “shell” and a massive core, the charge being distributed between the two and so, if the two are displaced relative to each other, giving rise to a dipole.

In the quasiharmonic approximation²⁰ it is assumed that the Helmholtz free energy of a crystal, F , at a temperature T can be written as the sum of static and vibrational contributions,

$$F(\mathcal{E}, T) = \Phi_{\text{stat}}(\mathcal{E}) + F_{\text{vib}}(\mathcal{E}, T) \quad (1)$$

Φ_{stat} is the potential energy of the static lattice in a given state of strain \mathcal{E} . Traditional static lattice simulations²¹ evaluate Φ_{stat} and neglect F_{vib} which is the sum of harmonic vibrational contributions from all the normal modes. For a periodic structure, the frequencies $\nu_j(\mathbf{q})$ of modes with wavevector \mathbf{q} are obtained by diagonalisation of the dynamical matrix $D(\mathbf{q})$.²² F_{vib} is given by

$$F_{\text{vib}} = \sum_{\mathbf{q}, j} \left\{ \frac{1}{2} h \nu_j(\mathbf{q}) + k_B T \ln[1 - \exp(-h \nu_j(\mathbf{q})/k_B T)] \right\} \quad (2)$$

in which the first term is the zero-point energy. For a macroscopic crystal the sum over \mathbf{q} becomes an integral over a cell in reciprocal space, which can be evaluated by taking successively finer uniform grids²³ until convergence is achieved. The free energy thus obtained is a function of both macroscopic (η_λ) and internal (ε_k) strains, and it is simplest to treat the ε_k as thermodynamic variables on the same footing as the η_λ , comprising a total set of strain variables^{24,25} denoted by \mathcal{E}_A . The equilibrium structure at an applied pressure, P_{ext} , is then that which minimises the availability²⁶ $\tilde{G} = F + P_{\text{ext}} V$ with respect to all strains. The number of independent degrees of freedom can often be reduced substantially by symmetry considerations.

The derivatives of $F + P_{\text{ext}} V$ can of course be carried out by brute force, from numerical values of F obtained using eqn.

(2). However, for large unit cells with many internal strains it is much more efficient to use analytic expressions for the derivatives of F with respect to temperature and strain. This not only leads to explicit expressions for thermodynamic properties, such as the entropy S ,

$$S = \sum_{q,j} \left\{ \frac{(hv_j(\mathbf{q})/T)}{\exp(hv_j(\mathbf{q})/k_B T) - 1} - k_B \ln[1 - \exp(-hv_j(\mathbf{q})/k_B T)] \right\} \quad (3)$$

which can be readily evaluated to a high precision; but in addition the strain derivatives permit a more rapid minimisation of $F + P_{\text{ext}}V$. The strain derivatives are given by

$$\left(\frac{\partial F_{\text{vib}}}{\partial \mathcal{E}_A} \right)_{\mathcal{E}', T} = \sum_{q,j} \left\{ \frac{h}{2v_j(\mathbf{q})} \times \left(\frac{1}{2} + \frac{1}{\exp(hv_j(\mathbf{q})/k_B T) - 1} \right) \left(\frac{\partial v_j^2(\mathbf{q})}{\partial \mathcal{E}_A} \right)_{\mathcal{E}'} \right\} \quad (4)$$

where the subscript \mathcal{E}' denotes that all the \mathcal{E} are kept constant except for the differentiation variable. We thus require derivatives of the frequencies. In our new code the derivatives $(\partial v_j^2(\mathbf{q})/\partial \mathcal{E}_A)_{\mathcal{E}'}$ are obtained from the analytic expressions for the derivatives $(\partial D/\partial \mathcal{E})_{\mathcal{E}'}$ by first-order perturbation theory. Full expressions for two and three-body short-range potentials and for the Ewald and Parry summations are given in refs. 27, 28 and 29. For obtaining derivatives the perturbation is infinitesimal and so the procedure is exact. Furthermore, for thermodynamic properties no special consideration needs to be given to degeneracies in first order perturbation theory, since the trace of $(\partial D/\partial \mathcal{E}_A)_{\mathcal{E}'}$ is invariant for any complete normal set of eigenvectors of D .

To obtain the equilibrium structure and Gibbs energy our new code uses a variable metric method³⁰ for minimising $F + P_{\text{ext}}V$ with respect to the \mathcal{E}_A . In the initial configuration the static energy Hessian, $(\partial^2 \Phi_{\text{stat}}/\partial \mathcal{E}_A \partial \mathcal{E}_B)$, which is a good approximation to $(\partial^2 F/\partial \mathcal{E}_A \partial \mathcal{E}_B)$, is calculated from its analytic expression, and its inverse together with the $(\partial F/\partial \mathcal{E}_A)$ is used to obtain an improved configuration. In subsequent iterations the $(\partial F/\partial \mathcal{E}_A)$ are calculated in the new configurations and the inverse Hessian updated by the BFGS formula.³¹ The exact details of the algorithm are given in ref. 15.

The quasiharmonic approximation breaks down with increasing amplitude of vibration and hence at high temperatures. This can be investigated either by computing terms in the lattice dynamics of higher order in the anharmonicity, or more commonly, as below, by classical MC or MD simulations. A general rule of thumb we have found useful for ionic solids is that the quasiharmonic approximation is usually valid up to temperatures of approximately one-half to two-thirds of the melting point. For any given temperature, higher pressures correspond to smaller internuclear separations and amplitudes of vibration so the breakdown of the quasiharmonic approximation is often less important for applications involving high pressure.

Monte Carlo

In the MC method, the properties of interest are evaluated from averages over a large number of configurations generated in phase space according to the prescribed probability function of the ensemble. In an MD simulation, the properties are computed through direct numerical integration of the classical Newtonian equations of motion of the particles constituting the system. In our MC work vibrational effects are taken into account by allowing random moves of randomly selected atoms. The MC calculations are carried out within

the NPT ensemble, *i.e.* both the atomic coordinates and cell dimensions were allowed to vary during the simulation. We briefly discuss the pertinent details of the calculation since detailed descriptions of the MC methodology are available in refs. 3 and 32. During one step of the MC simulation an atomic coordinate or a lattice parameter is chosen at random and altered by a random amount. To determine whether the change is accepted or rejected, the usual Metropolis algorithm is applied. The maximum changes in the atomic displacements and the lattice parameters are governed by the variables r_{max} and v_{max} respectively. There are separate values of r_{max} for each atom type and the magnitude of the displacements are adjusted automatically during the equilibration part of the simulation to maintain an acceptance/rejection ratio of approximately 0.3. The values of v_{max} for each lattice parameter are adjusted in a similar way.

Molecular dynamics

We have also carried out MD simulations at constant pressure and temperature based on an extended system as described in ref. 33. Constant NVE runs of 10 ps gave initial configurations, which were used as the starting point for equilibration runs at constant NPT of 10 ps, followed by production runs of 10 ps for each pressure and temperature considered, using a timestep of 1 fs. The temperature and pressure were kept constant by using an extended system with thermostat and barostat relaxation times of 1 and 0.5 ps respectively. The reliability of the results was checked by selected further runs with simulation times longer than 10 ps.

Hybrid methods

For solids with a high impurity content and solid solutions, we have recently developed a hybrid Monte Carlo (HMC) method,³⁴ combining MC and MD steps in the same simulation. The motivation for this has been the extensive use made by related techniques in the modelling of polymers and biomolecules.³⁵

A key feature is the sampling of many different configurations, allowing the exchange of ions located at crystallographically inequivalent positions. In our simulations this is achieved by an explicit interchange of the positions of these ions. A further major problem is the development of ways for taking into account the complex movements (relaxation) of large numbers of ions which accompany this exchange of ions (*e.g.*, Mn^{2+} and Mg^{2+}). Otherwise energy barriers are so large that all trial moves are rejected.³⁴ We do not resort to any parameterisation scheme or approximate Hamiltonian which averages out *local* effects due to ion clustering and association. The use of parameterised Hamiltonians (of *e.g.*, the Ising-type) has proved problematic for oxides and silicates and is not readily extended to incorporate the effects of high pressure or thermal effects.

The HMC technique allows efficient sampling of a large number of different configurations. During one HMC cycle, one of three options is chosen at random, with equal probability. The first is a short NVE molecular dynamics simulation (15 steps, timestep 1.5 fs) in which the last configuration is accepted or rejected by comparing its energy with the energy of the starting configuration and using the standard Metropolis algorithm. If the last configuration is rejected, the original configuration is included in the statistical averaging of thermodynamic properties. In the second option, which is only applicable to the solid solution, a short MD run follows a random exchange of atoms. Again, the difference in energy between the previous configuration and that immediately after the MD simulation is used in the Metropolis algorithm. At the start of each MD run, velocities are chosen anew at random from a Maxwellian distribution. The third option is a

random change of the volume/shape of the box³⁶ which again is accepted or rejected using the Metropolis algorithm.

We have also developed a configurationally averaged lattice dynamics approach to solid solutions³⁷ which involves the evaluation of an appropriate thermodynamic average over a (limited) set of calculations representing different arrangements of the cations within a supercell. Computational resources have normally restricted previous workers to assume just one (usually the most regular) arrangement and calculate its energy, with or possibly without relaxation.³⁸ Given the free energy, G_k , for the optimised structure of each possible cation arrangement k , obtained as described earlier, we then average so that

$$\langle H \rangle = \frac{\sum_k H_k \exp(-G_k/k_B T)}{\sum_k \exp(-G_k/k_B T)} \quad (5)$$

and

$$\langle S \rangle = \frac{\sum_k H_k \exp(-G_k/k_B T)}{T \sum_k \exp(-G_k/k_B T)} + k_B \ln \sum_k \exp(-G_k/k_B T) \quad (6)$$

Applications

MgF₂

We start with a straightforward example and consider selected thermodynamic properties of the rutile phase of MgF₂, the most stable at low pressure, using potentials derived from a calculated HF potential energy hypersurface, as described elsewhere.³⁹ We concentrate on the lattice parameters and thermal expansion. We have carried out QLD calculations, and MD and MC simulations. The last two used a simulation cell containing 192 Mg and 384 F ions arranged initially in a box of sides $4 \times 4.52 \text{ \AA}$, $4 \times 4.52 \text{ \AA}$ and $6 \times 3.09 \text{ \AA}$. In the MC simulations, the thermodynamic data were collected over 10^7 steps, prior to which a 10^7 step equilibration was carried out.

It is well known that the HF method generally overestimates lattice parameters,^{2,6} and for MgF₂ the HF lattice parameters a and c are slightly larger than experiment.⁴⁰ Fig. 1(a) and 1(b) show that the same conclusion applies to the values predicted using the new potential obtained by fitting to the HF energies. However, the variation with T of the lattice parameters a and c , calculated from QLD, MC, and MD are close to experiment (as shown in Fig. 1(a) and 1(b)). Below the Debye temperature (Θ_D), the MC values for a and c are slightly lower than the QLD values because only the latter takes account of quantum effects (largely zero-point vibration) which expand the lattice by a small amount. The MC and MD results are in good agreement.

The contribution of quantum effects in QLD can be assessed by removing such effects from the QLD calculations. This is readily achieved by replacing eqn. (2) with the high-temperature limiting expansion for the vibrational contribution to the free energy, *i.e.*, putting

$$F_{\text{vib}} = k_B T \sum_{q,j} \ln(h\nu_j(q)/k_B T). \quad (7)$$

Making this change, we obtain results below Θ_D which are in good agreement with those obtained from the MC and MD simulations, showing that the contribution of further anharmonic effects below Θ_D is very small.

At temperatures higher than the Debye temperature quantum effects play a less important rôle and there is a range of temperatures around Θ_D where the QLD and MC results are in good agreement. At high temperatures the MC results serve as a check of the validity of the quasiharmonic approximation. The QLD results show a characteristic divergence of slope from the MC results for $T \geq 1300 \text{ K}$, indicating that this

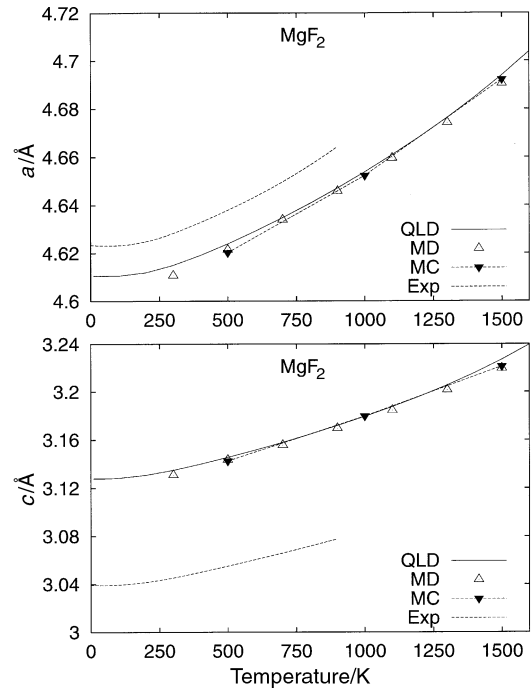


Fig. 1 Calculated temperature variation of a and c for MgF₂. Results from quasiharmonic lattice dynamics (QLD), Monte Carlo (MC) and molecular dynamics (MD) calculations are shown together with experimental data from ref. 40.

approximation is beginning to break down. Below this upper limit, it is clear that the Gibbs free energy can be calculated efficiently and accurately from lattice statics and QLD, without resorting to lengthy thermodynamic integration.

Simulations are a valuable means of examining critically common approximations, made for instance in geophysics, regarding the temperature and pressure dependence of important physical properties. For example, one widely used quantity is the isothermal Anderson–Grüneisen function, δ_T , given by

$$\delta_T = -(\partial \ln K_T / \partial \ln V)_P = -(\partial \ln \beta / \partial \ln V)_T \quad (8)$$

where β is the volumetric thermal expansion coefficient ($= (\partial V / \partial T)_P / V$) and K_T the isothermal bulk modulus. For the rutile phase of MgF₂ over its entire pressure range, we find that β is approximately proportional to V^t at 300 K, where $t \approx 7$, so giving δ_T a constant value of 7. For the fluorite phase adopted at high pressure,³⁹ in contrast, δ_T decreases with pressure from ≈ 5.7 at the transition to ≈ 4.7 at 80 GPa, still higher than the value of $\delta_T \approx 3$ deduced by D. L. Anderson⁴¹ from seismic data for the lower mantle, but in agreement with the observation of O. L. Anderson that δ_T decreases at high pressures. For comparison, the corresponding theoretical⁴² and experimental⁴³ value for MgO is $t \approx 6$. The calculated value of β for MgF₂ is larger for the fluorite phase than for the rutile phase. At 500 K, β increases by over a factor of 2 at the phase transition, as shown in Fig. 2. Consequently, due to the phase change, there is no marked decrease of β with pressure for MgF₂ (*cf.* MgO where there is no phase transition over the range of pressures considered here). Chopelas and Boehler⁴⁴ have discussed the implications of large values of δ_T for minerals.

Negative thermal expansion—ZrW₂O₈

A somewhat more complex example is that of ZrW₂O₈. This is of particular current interest^{45,46} since it exhibits large *negative* thermal expansion from 0.3 to 1050 K. At 428 K this material undergoes a phase transition to a disordered phase,

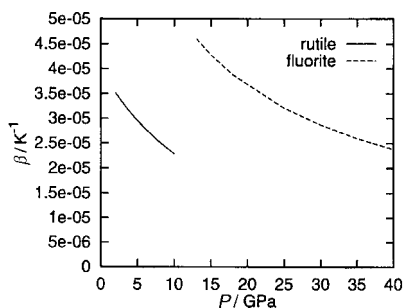


Fig. 2 Calculated variation of the thermal expansion coefficient β at 500 K with pressure for the rutile and fluorite phases of MgF_2 .

but below this temperature the well-ordered structure provides an excellent test of our methodology. Fig. 3 shows that the unit cell of ZrW_2O_8 is cubic and composed of WO_4 tetrahedra sharing corners and ZrO_6 octahedra linked in such a way that each octahedron shares corners with six different WO_4 tetrahedra. Each WO_4 tetrahedron shares only three of its four oxygens with adjacent ZrO_6 octahedra.

We have carried out lattice statics and QLD calculations for ZrW_2O_8 analogous to those for MgF_2 . For the intraoctahedron O–Zr–O and intratetrahedron O–W–O interactions, we have chosen to use a Urey–Bradley term of the form,

$$E = \frac{1}{2}k(r_{\text{O-O}} - r_e)^2 \quad (9)$$

where $r_{\text{O-O}}$ is the oxygen–oxygen distance and r_e a constant, rather than a standard harmonic angle term. A similar type of forcefield has been used recently for silicates with success by Gale.¹⁷ Our calculated value for the linear thermal expansion coefficient α ($= \beta/3$) over the range 50–300 K is -3.5×10^{-6} which compares with the observed value⁴⁶ of $\approx -8.3 \times 10^{-6}$.

To understand why negative thermal expansion is associated with this type of cubic structure, it is useful to express the volumetric expansion coefficient, using a Maxwell relation, in terms of $(\partial S/\partial V)_T$:

$$\beta = \chi_T(\partial S/\partial V)_T \quad (10)$$

where χ_T is the isothermal compressibility. Since χ_T is always positive, then β and $(\partial S/\partial V)_T$ have the same sign. $(\partial S/\partial V)_T$ is negative for ZrW_2O_8 largely due to the Zr–O–W transverse vibrations, which increase in frequency with increasing Zr–W

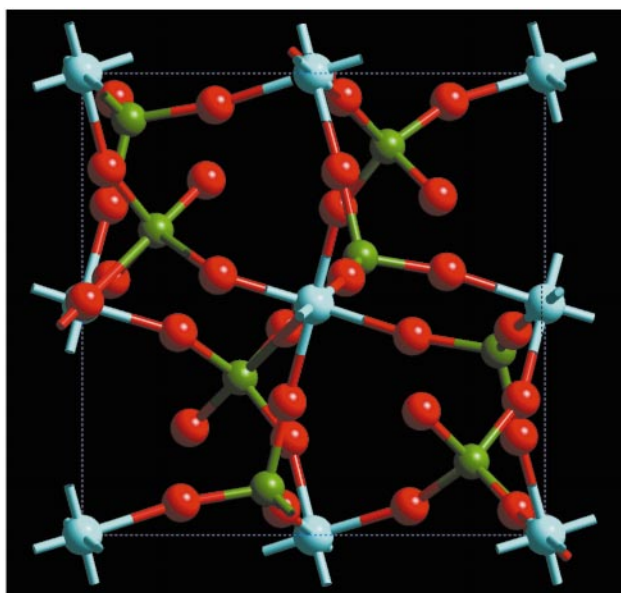


Fig. 3 Room temperature structure of ZrW_2O_8 . Zr atoms are light blue, W are green and O are red.

internuclear separation (*cf.* the transverse vibrations of a stretched violin string). This tension effect⁴⁷ dominates, in general, only in open, framework structures. A useful and related treatment of the negative thermal expansion in this system in terms of “rigid unit modes”, *i.e.*, low-frequency phonon modes which propagate with no distortion of the ZrO_6 octahedra or WO_4 tetrahedra, has been given by Pryde *et al.*⁴⁸ Negative thermal expansion is reviewed more extensively in ref. 49.

At pressures over 0.2 GPa, cubic ZrW_2O_8 undergoes a phase transition to an orthorhombic phase,⁵⁰ with a $\approx 5\%$ reduction in cell volume. In this less open structure the average W and O coordination numbers are increased due to enhanced interactions between adjacent WO_4 groups. The decreased flexibility is reflected in calculated and observed expansion coefficients an order of magnitude smaller than for the cubic phase.

In this context it is also worth noting the work of Parker *et al.* who, using numerical derivatives of the free energy, predicted negative thermal expansion coefficients for certain crystalline zeolite framework structures.⁵¹ These have subsequently been confirmed experimentally.⁵²

Surface free energies

Though there have been many simulations of surfaces which have considered only the static contribution to the total energy of the relaxed surface,^{53–55} few studies have included dynamic effects, including temperature. Molecular dynamics has been used to study the {001} surfaces of KCl ⁵⁶ and NiO ,⁵⁷ and Mulheran and co-workers have used a localised Einstein-like approximation^{58,59} for the phonon spectrum to estimate the temperature dependence of surface energies.

Here we present results based on the full minimisation of the free energy for the {001} and {110} surfaces of MgO . Irregularities such as ledges, kinks, steps, and electronic defects, present on real surfaces, are ignored. The well-established set of shell-model interionic potentials for MgO due to Stoneham and Sangster⁶⁰ is used. Our strategy differs substantially from the two-region strategy commonly used for static calculations,^{53,55} where only the positions and polarizations of the ions in the vicinity of the surface are relaxed explicitly while the remainder are constrained to their bulk lattice positions. We consider a slab in which the crystal is infinite in two directions and finite in the other. If the slab is sufficiently thick to provide effectively a bulklike region in the interior of the slab, then the two surfaces, essentially noninteracting, can be taken as free surfaces.

Fig. 4 shows the calculated temperature dependence of the {001} surface energy of MgO . Approximately 10 layers are sufficient to achieve convergence to 0.001 J m^{-2} . This is more than twice the number of layers necessary for the convergence of the static energy. The {001} surface energy decreases with temperature, less markedly than predicted for the {001}

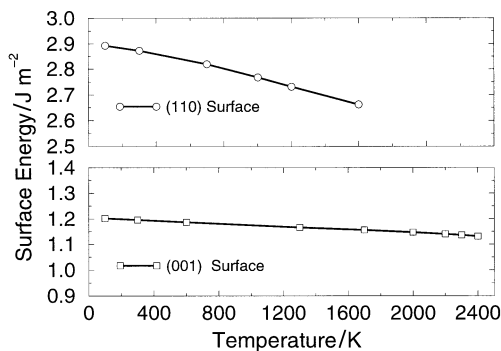


Fig. 4 Calculated temperature variation of the surface energies of the {001} and {110} surfaces of MgO .

surface of NiO by Mulheran.⁵⁹ The variation with temperature is consistent with that noted for rocksalt (100) surfaces by Benson and Yun.⁶¹

The {110} surface shows a rather more marked decrease with temperature than the {001}, as is clear from Fig. 4. For this surface, at ≈ 1600 K the quasiharmonic approximation breaks down when imaginary frequencies appear. The analogous temperatures for the appearance of imaginary frequencies in the bulk and the {001} surface are ≈ 2900 K and ≈ 2600 K respectively; indicating that the quasiharmonic approximation fails at somewhat lower temperatures for the surfaces than for the bulk modes, due to modes with large amplitude of vibration. It is tempting to suggest that surface melting occurs at temperatures below that of the bulk (3100 K).

Fig. 5 shows calculated bulk, surface and surface-excess phonon densities of states for these two surfaces of MgO at 700 K. The surface calculations were carried out on slabs fully relaxed at this temperature. Also plotted is the excess DOS (surface minus bulk) which is responsible for the dynamic contribution to the surface free energies. The appearance of surface-localized modes is clear and the intensity of some important bulk modes decreases. The excess DOS for the {100} surface is in good agreement with experiment⁶² up to ≈ 18 THz. The calculations do not show the peak reported above 18 THz and so do not support an earlier suggestion⁶³ that surface relaxation at elevated temperature is responsible for this feature. One possible explanation²⁹ for the peak at high frequencies is the presence of steps on the {100} surface, which can alternatively be described as the formation of a microfaceted {110} surface. Refs. 29 and 64 contain results for a wider range of oxide surfaces.

Defect energies and defect volumes

Our next example is the substitution of Mg^{2+} in MgO by Ba^{2+} , which involves a large structural distortion of the lattice since the Ba^{2+} ion is so much larger than Mg^{2+} . A detailed study of the defect free energies, enthalpies and volumes over the range 0–1500 K, which to our knowledge is the first report

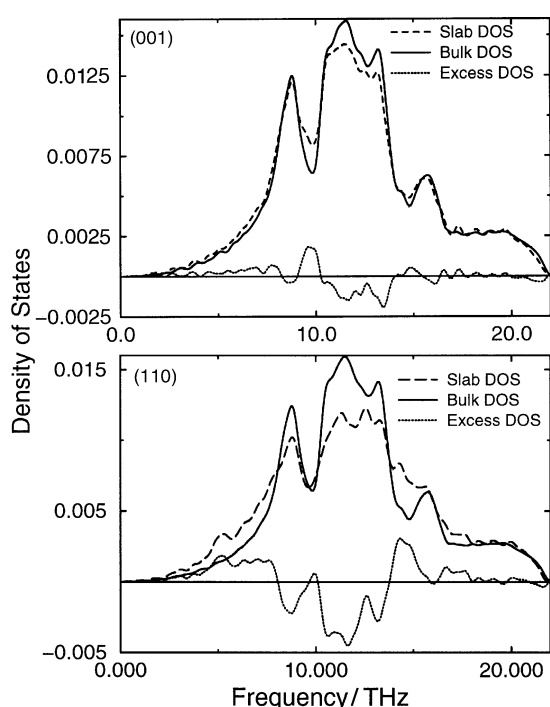


Fig. 5 Calculated bulk, and {001} and {110} surface-excess (surface-bulk) phonon densities of states at 700 K for MgO.

based on the full minimisation of all internal and external strains, has been given previously.⁶⁵

The approach we use here is based on the well-established use of “supercells” to describe the defective lattice. A superlattice of defects is introduced extending throughout the macroscopic crystal. The periodicity is then of the superlattice and the supercell contains many atoms whose equilibrium positions are not wholly determined by symmetry, but are described by a set of dimensionless internal strain coordinates ϵ_k . Defect properties such as energies and entropies, which are denoted by lower case letters (*e.g.*, g_p denotes the change in Gibbs free energy at constant pressure) can then be computed both at constant pressure and at constant volume, *e.g.*,

$$f_v = f_v(V, T) = \{F_{dc}(V, T) - F_{pc}(V, T)\}/N_d \quad (11)$$

$$g_p = g_p(P, T) = \{G_{dc}(P, T) - G_{pc}(P, T)\}/N_d \quad (12)$$

$$u_v = u_v(V, T) = \{U_{dc}(V, T) - U_{pc}(V, T)\}/N_d \quad (13)$$

$$h_p = h_p(P, T) = \{H_{dc}(P, T) - H_{pc}(P, T)\}/N_d \quad (14)$$

where the subscripts dc and pc refer to the defect crystal and perfect crystal respectively and quantities in capital letters are free energies (F , G), internal energies (U) or enthalpies (H) of the macroscopic crystal. N_d is the total number of defects introduced into the macroscopic crystal. No account therefore is taken here of the configurational entropy of randomly positional defects in the lattice, which is of course asymptotically correct for a single isolated defect. Convergence towards properties of an isolated defect occurs as the superlattice spacing is increased.

We calculate directly the free energy changes accompanying defect formation at constant pressure (g_p) and constant volume (f_v). To calculate f_v , the external strain is kept constant while the internal degrees of freedom are varied to give the equilibrium configuration at temperature T . Similarly, for g_p , both external and internal strains are varied to be consistent with the specified pressure. It is straightforward to determine u_v and h_p from the terms that contribute to f_v and g_p . The volume of formation of the defect, v_p , follows immediately from the minimisation of $F + P_{\text{ext}}V$.

We show in Fig. 6 the variation of h_p and u_v with temperature, calculated using lattice dynamics, for a supercell of 216 ions, containing one Ba ion. $h_p(T)$ is always greater than $u_v(T)$ above $T = 0$; in the isolated defect limit, it is possible to show⁶⁶ that

$$h_p - u_v = (\beta T/\chi_T)v_p \quad (15)$$

Here both β and v_p are positive. Fig. 6 shows that the temperature dependence of u_v is much larger than that of h_p and opposite in sign. The results confirm the traditional assumption^{66,67} that $u_v(0)$ and $u_v(\text{static})$ are fair approx-

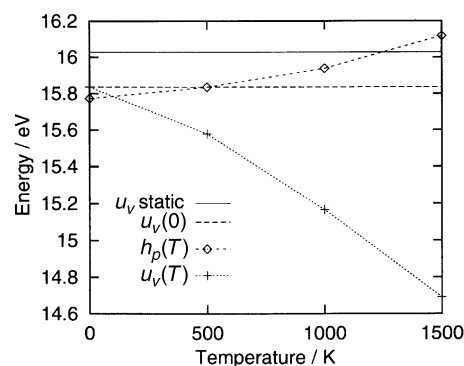


Fig. 6 Temperature variation of h_p (\diamond) and u_v (+) for a supercell containing 216 ions. For comparison $u_v(0)$ and $u_v(\text{static})$ are also shown.

imations to $h_p(T)$. $u_v(\text{static})$ is a better approximation when $T > \Theta_D$. While the high temperature values of u_v clearly extrapolate back towards $u_v(\text{static})$, the same is not true of h_p .

In Fig. 7 we compare the results for h_p and v_p calculated using lattice statics and QLD with those obtained from subtracting the results of (NPT) MC simulations on the defective and the perfect crystals. The MC simulations are at least two orders of magnitude more expensive than the lattice dynamics calculations. The uncertainties in the MC calculation are such that the precision of the MC results is much less than those from lattice dynamics. Nevertheless the two sets of results in Figs. 6 and 7 are entirely consistent. Where, as here, the thermodynamic quantity of interest is determined by the relatively small difference between two large quantities ($h_p \approx 16$ eV which compares with an enthalpy of ≈ 4400 eV for a supercell of 216 ions), the high precision of the lattice dynamics approach is particularly valuable.

Solid solutions

Disorder in polar solids has largely been investigated theoretically *via* point defect calculations, which refer only to the dilute limit, or as in the previous section *via* supercells. These methods are not readily extended to mixtures or disordered systems containing a finite impurity or defect content. Modelling studies have thus focused on problems involving low concentrations of defects. This is particularly unfortunate due to the evident experimental importance of disordered and grossly non-stoichiometric systems.

In Fig. 8 we show the values of ΔH_{mix} for MnO/MgO determined using our HMC technique and a box-size of 216 ions at 1300 K, with a set of interionic potentials taken from ref. 68,

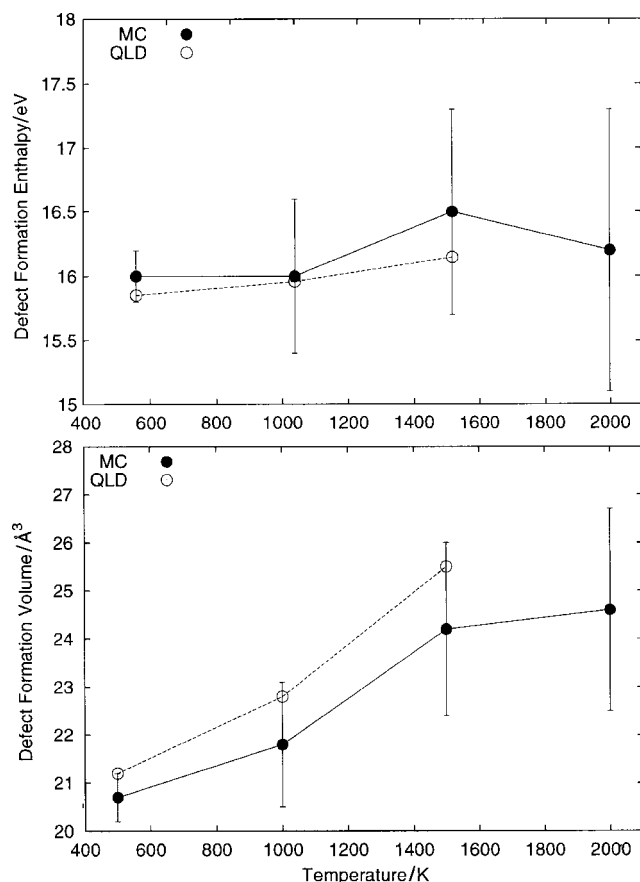


Fig. 7 Temperature variation of h_p and v_p for a substitutional Ba defect in MgO calculated from Monte Carlo (MC) and quasi-harmonic lattice dynamics (QLD) simulations. The error bars show the root mean square deviations in the calculated quantities.

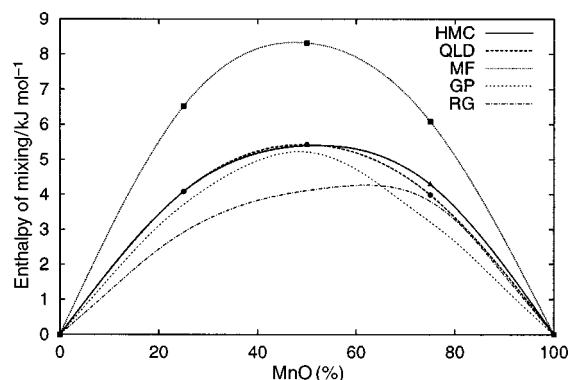


Fig. 8 Calculated values of ΔH_{mix} at 1300 K for MnO/MgO using hybrid Monte Carlo (HMC), mean field theory (MF) and quasi-harmonic lattice dynamics (QLD). Two sets of experimental data are also shown (RG from ref. 71, GP from ref. 70).

20000 equilibration cycles and 20000 data collection steps. We also show values calculated using a mean field (MF) treatment. Here, instead of distinct Mg^{2+} and Mn^{2+} ions, a “hybrid” ion is introduced, for which the non-Coulombic potentials are a linear combination of the potentials for Mn^{2+} and Mg^{2+} , weighted appropriately by the site occupancies. If local relaxation or clustering is important, then mean-field results will be poor. Fig. 8 shows that this is the case even in our relatively straightforward example with two cations not too dissimilar in size (sixfold coordinate radii are 0.83 Å and 0.72 Å for Mn^{2+} and Mg^{2+} respectively⁶⁹). It is worth stressing that here traditional Monte Carlo and traditional molecular dynamics, excluding explicit interchange of cations, failed completely as a negligible number of Mn and Mg interchanges took place, highlighting the need for methods in which different configurations are sampled efficiently. A comparison of methods for achieving this sampling in a range of different systems is given in ref. 34.

In Fig. 8 we also show the values of ΔH_{mix} for MnO/MgO determined using configurationally averaged lattice dynamics and eqn. (5), with a unit cell of 64 atoms and 32 randomly-chosen cation arrangements. In this case the cell size and the number of cation arrangements is sufficient to ensure convergence in ΔH_{mix} to 0.1 kJ mol⁻¹. It is clear from Fig. 8 that there is excellent agreement between the QLD and HMC methods. The enthalpy of mixing at 1300 K is symmetric with a maximum of approximately 5.4 kJ mol⁻¹ (50% MgO, 50% MnO). Agreement with the data of Gripenberg *et al.*⁷⁰ is good; we see none of the asymmetry reported by Raghavan.⁷¹ The calculated value of ΔH_{mix} varies only slightly with temperature.

The lattice dynamics approach is particularly useful for quantities such as entropies of mixing since free energies are calculated so readily. Fig. 9 shows entropies of mixing for CaO/MgO (for mole fractions of CaO less than 0.15), calculated using eqn. (6). The size mismatch⁶⁹ between the two different cations is greater (1.00 and 0.72 Å) than for MnO/MgO. Results are for cell sizes of 54, 64, 72 or 96 atoms and 95 randomly chosen configurations. The corresponding figure for 120 configurations is indistinguishable by eye. ΔS_{mix} includes both configurational and vibrational contributions; no assumptions are made regarding the ideality or otherwise of the solid solution. As with the isolated barium substitutional defect in MgO discussed earlier the vibrational contribution is positive since it is dominated by the heavier mass of the impurity ion which tends to decrease frequencies and the overall ΔS_{mix} is larger than the “ideal” value.

A valuable feature of hybrid MC is that it can be readily used to examine the influence of high impurity or defect concentrations on phase transitions. Alternative methods such as the use of an Ising-type Hamiltonian can not only average out

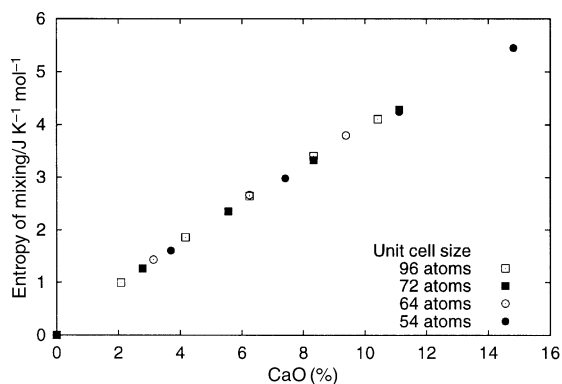


Fig. 9 Calculated values of ΔS_{mix} at 1800 K for CaO/MgO calculated using lattice dynamics.

local effects such as ion association but are not readily extended to include the effects of lattice vibrations and high pressure. Since Mn–Mg mixing in silicates is expected to be quite non-ideal,⁷² we have chosen to examine (Mg, Mn)SiO₃ perovskite.⁷³ Parameterisation of approximate Hamiltonians becomes increasingly difficult for such compounds beyond binary or pseudobinary mixtures.

We used the same set of interionic potentials for MgSiO₃ as for Mg₂SiO₄ in ref. 34. The HMC runs are for a simulation cell of 540 ions ($3 \times 3 \times 3$ unit cells), with an equilibration period of 50 000 cycles and averaging enthalpy and structural data over a further 50 000 cycles. Matsui and Price⁷⁴ have used constant-pressure molecular dynamics to show that above 10 GPa, orthorhombic MgSiO₃ undergoes a temperature induced phase transition to a cubic phase prior to melting, whereas at lower pressures the orthorhombic phase melts without any change of solid phase. For MgSiO₃ itself, HMC results are very similar. The calculated transition temperature from the orthorhombic to the cubic phase is 3900 K at 20 GPa. Fig. 10(a) shows the variation of the lattice parameters of Mg_{0.6}Mn_{0.4}SiO₃ with temperature, which shows this

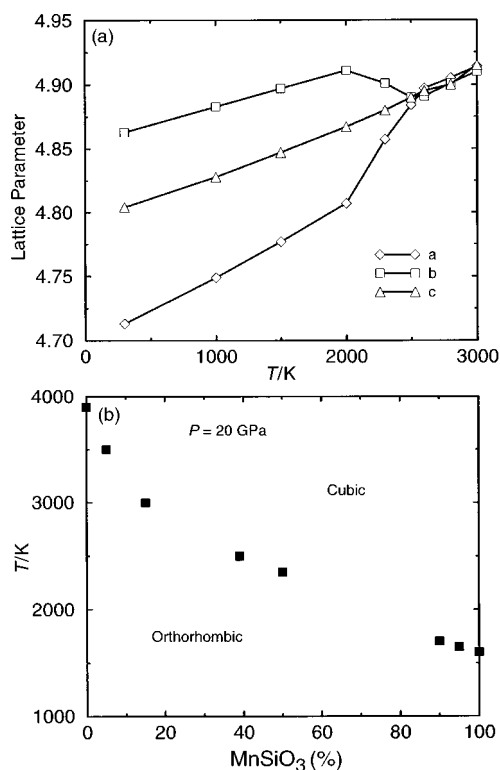


Fig. 10 (a) Lattice parameters (Å) vs. T (K) at 20 GPa for Mg_{0.6}Mn_{0.4}SiO₃. (b) Calculated orthorhombic–cubic transition temperature (K) at 20 GPa vs. Mn content.

compound also undergoes such a phase transition at this temperature. The transition temperature (2500 ± 50 K) is lower than for MgSiO₃, in keeping with simple radius ratio arguments. The calculated transition temperature at 20 GPa as a function of Mn composition is displayed in Fig. 10(b), and it is evident that a linear interpolation between the end members is a very poor approximation. The orthorhombic–cubic phase transition for Mg_{0.6}Mn_{0.4}SiO₃ is 500 K lower than the value of ≈ 3000 K predicted by such an interpolation. In passing, it is worth noting that, unlike the transition temperature, the calculated volume as a function of Mn composition shows only a small positive deviation from Vegard's law, since the a lattice parameter has a positive deviation and the other two negative deviations. We have not been able to find experimental data for comparison; data are particularly sparse where a combination of high temperatures and high pressures is required. If the analogous compound (Mg, Fe)SiO₃ were to exhibit such a phase transition⁷⁵ there would be important implications for the thermodynamic and compositional modelling of the Earth's mantle.

Mechanisms

Most of this feature article has been devoted to thermodynamic properties. Somewhat surprisingly, little attention appears to have been paid in the literature to calculations related to kinetic and mechanistic aspects. Accordingly we present here a study of the activation energies of possible mechanisms for the B1–B2 transition at high pressure. This is of considerable interest as a model for other structural phase transformations, including those of geophysical importance, as it is one of the simplest first-order non-displacive transitions (see, *e.g.*, refs. 76, 77).

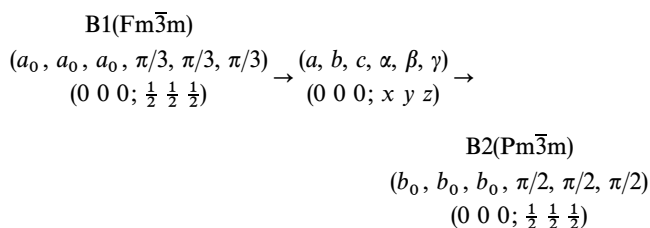
Experimentally there appear to be large energy barriers to the B1–B2 transformation. In large, pure crystals the transformation occurs suddenly and simultaneously over the entire crystal volume.⁷⁸ The B1 crystal must be subjected to a pressure larger than the thermodynamic transition pressure P_{trans} in order to obtain the B2 phase. In the reverse direction a pressure lower than P_{trans} is required. The B2 \rightarrow B1 transition in CsCl at 718 K and zero pressure has also been investigated by X-ray studies of single crystals and optical microscopy of single crystals.⁷⁹

A structural phase transition of a macroscopic crystal involves the movement of a number of atoms of the order of Avogadro's constant, N_A , and, in principle, a potential energy hypersurface of $\sim 3N_A$ dimensions. For the purposes both of defining possible mechanisms, *i.e.* specific atomic pathways, and their practical calculation, the number of dimensions must clearly be reduced to only a few. This is achieved most simply by assuming that some degree of periodicity is retained in the course of the transition and hence that the mechanism of the transition can be defined in terms of the size and symmetry of the repeat unit connecting the two phases. Retention of periodicity implies that the phase transition is a cooperative process involving a concerted movement of atoms with no account taken of the possible rôle played by defects.

Since the repeat unit can be constructed from multiple unit cells ranging from single unit to $\sim N_A$ -unit cells, all possible mechanisms can be defined in terms of the size of the repeat unit and one of the common sub-groups which define its symmetry. Thus all mechanisms can be indexed as $M(n, S)$, where n corresponds to the number of atoms in the repeat unit and S the symmetry. It follows that the dimensions of the corresponding potential energy hypersurfaces also depend on the size and symmetry of the repeat unit.

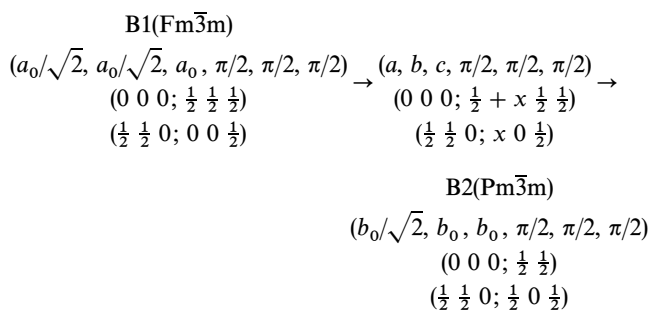
The B1–B2 transformation has been discussed chiefly in the context of two possible mechanisms. The first, often the only model presented in standard texts,⁸⁰ was proposed initially by Shoji⁸¹ and subsequently modified by Buerger.⁸² We refer to

this as the Buerger mechanism; it involves a simultaneous increase of the rhombohedral angle of the primitive B1 crystallographic cell and a change in the lattice parameter. Thus for a two ion repeat unit, writing the transition in terms of the unit cell variables ($a, b, c, \alpha, \beta, \gamma$) and irreducible atomic positions $(0\ 0\ 0; x\ y\ z)$:



In our notation the Buerger mechanism corresponds to $M(2, R\bar{3}m)$. Fig. 11 (also see ref. 83†) shows the deformation of the B1 cell towards B2 in this mechanism. Lower symmetry variants which retain a two-atom unit cell are discussed by Gufan and Ternovskii⁸⁴ and Sims *et al.*⁸⁵

A second possibility was introduced by Watanabe, Tokonami and Morimoto⁷⁹ (WTM) in their study of the $B2 \rightarrow B1$ transition in CsCl. It involves a concerted translation of adjacent planes relative to one another with simultaneous rearrangements of the ions within each plane. It corresponds to a four-atom orthorhombic repeat unit which transforms as $Pmm2$ (25), *i.e.* $M(4, Pmm2)$. The transition can be represented as



The WTM mechanism is somewhat more difficult to visualise since it involves both the intralayer rearrangement of ions and the translation of these layers relative to one another. The details are shown in Fig. 12. Referring to the lattice vectors marked in this figure, the B2 structure is generated from the B1 structure by increasing the b/a ratio from $b = a$ to $b =$

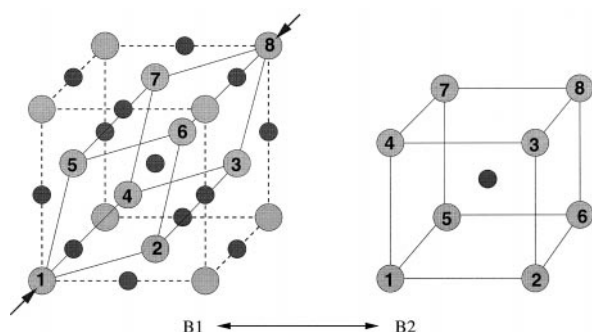


Fig. 11 Buerger mechanism for the conversion of the B1 into the B2 phase. The figure shows primitive unit cells. See also ref. 83.

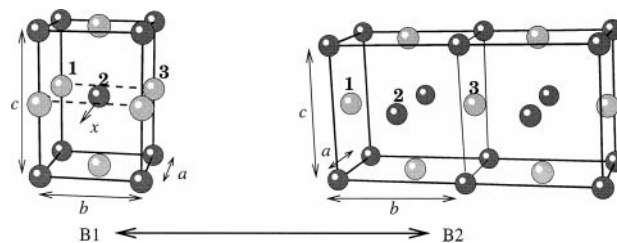


Fig. 12 WTM mechanism for the conversion of the B1 into the B2 phase. For the B1 phase the a - and b -lattice vectors marked lie in the $\{100\}$ plane of the conventional unit cell.

$a\sqrt{2}$. Simultaneously every alternate (001) plane (the label (001) refers to the B1 structure throughout) is displaced by an amount x in the a -direction, as illustrated also in Fig. 12; x is in units of a . The magnitude of the spacing of the (001) planes, c , also changes. The (001) and $(\bar{1}10)$ planes of the B1 structure become the (011) and $(0\bar{1}1)$ planes, respectively, of the B2 structure. We have a four parameter space, denoted here by the magnitudes of the three lattice vectors a, b, c and x where x is the magnitude of the slip of the (001) planes. Although $a\sqrt{2} = c$ for both B1 and B2 structures this is not necessarily so for every point on the minimum energy pathway. Clearly, calculations involving the WTM mechanism are more costly than those for the Buerger mechanism.

Here we present results for SrO, calculated using CRYSTAL95⁶ with the Hay and Wadt small core pseudopotential,¹⁰ as used previously.¹¹ To our knowledge this is the first report where the two mechanisms have been compared using *ab initio*, rather than pair-potential, methods.

We start by calculating the variation of G with P for both the B1 and B2 phases. The electronic energy Φ_{stat} was determined for a range of volumes, V , and the corresponding pressure, evaluated numerically from $-(d\Phi_{\text{stat}}/dV)$. In the static limit the Gibbs energy, G , equals the enthalpy, H , and so

$$\begin{aligned} G &= H = \Phi_{\text{stat}} + PV \\ &= \Phi_{\text{stat}} - V(d\Phi_{\text{stat}}/dV) \end{aligned} \quad (16)$$

The thermodynamic transition pressure between any two phases is the pressure at which the Gibbs energies of the two phases are equal, *i.e.*,

$$G_{\text{B1}}(p, V_{\text{B1}}) = G_{\text{B2}}(p, V_{\text{B2}}) \quad (17)$$

For SrO the calculated B1–B2 transition pressure is 31.7 GPa, which compares with an experimental value⁸⁶ of 36 ± 4 GPa.

Turning to the possible pathways between the B1 and B2 structures, we have determined the \tilde{G} surface in the static limit, where $\tilde{G} = \Phi_{\text{stat}} + P_{\text{ext}}V$ for both Buerger and WTM mechanisms. Fig. 13 shows, for the Buerger mechanism, a plot of the calculated \tilde{G} surface as a function of a and α for SrO with $P_{\text{ext}} = P_{\text{trans}}$ (*i.e.*, with the external pressure equal to the thermodynamic transition pressure). This shows two minima at the points corresponding to the B1 and B2 phases. Using standard procedures,³¹ it is straightforward to determine the minimum energy pathway between the two phases, and this is shown in Fig. 13(b), as a function of reaction coordinate s , which we label using the corresponding value of α . There is a clear activation energy barrier of ≈ 29 kJ mol⁻¹ at this applied pressure (P_{trans}). Fig. 13(c) indicates the variation of a and α corresponding to the minimum energy pathway of Fig. 13(b); a decreases as the rhombohedral angle α increases and the cell opens out.

Visualisation is more complicated for the WTM pathway for SrO because more variables must be considered and we simply quote the final results. Just as for the Buerger mechanism, at $P_{\text{ext}} = P_{\text{trans}}$ the WTM mechanism is also an activated

† Available as electronic supplementary information. See <http://www.rsc.org/suppdata/cp/a9/a908622f>

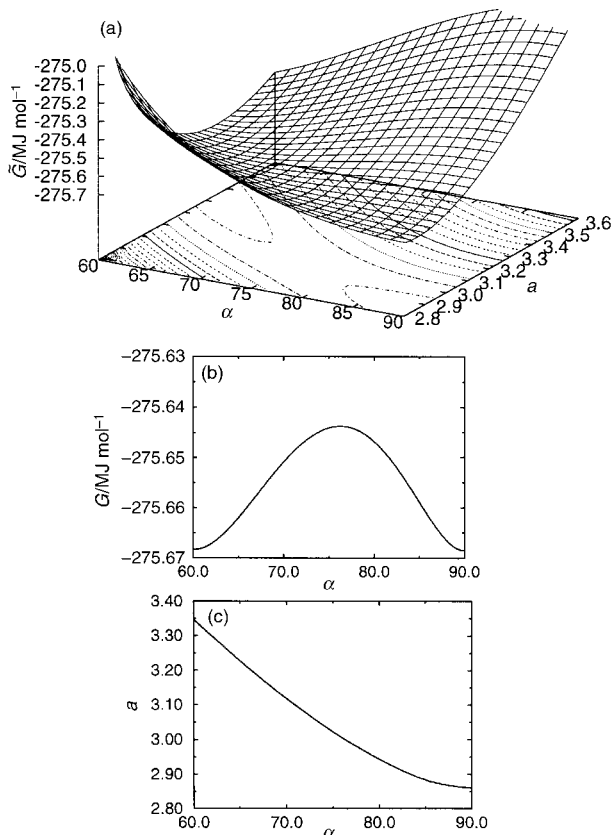


Fig. 13 (a) Calculated free energy surface (\bar{G}), in the static limit, for the Buerger mechanism in SrO. $P_{\text{ext}} = P_{\text{trans}}$. Energy (MJ mol^{-1}) is plotted as a function of a (\AA) and α (degrees). (b) Calculated minimum energy pathway for the Buerger mechanism in SrO, as a function of reaction coordinate s , which we label using the corresponding value of α . $P_{\text{ext}} = P_{\text{trans}}$. (c) Variation in a (\AA) and α (degrees) along the pathway in part (b).

process, with a lower barrier of $\sim 20 \text{ kJ mol}^{-1}$. Although $c/a = \sqrt{2}$ at the end points of the transition, this ratio does not remain constant during the transition. The activation energies for the two mechanisms are similar in magnitude to those found in ref. 85 using a two-body potential model (17 kJ mol^{-1} and 20 kJ mol^{-1} for Buerger and WTM mechanisms respectively) but the relative order is reversed. The *ab initio* results presented here suggest the transition takes place *via* the WTM mechanism. The calculated *ab initio* activation volumes, defined as the difference between the volume (per formula unit) of the transition state and that of the equilibrium B1 structure, at the transition pressure, is $-9.08 \times 10^{-7} \text{ m}^3 \text{ mol}^{-1}$ and $-8.92 \times 10^{-7} \text{ m}^3 \text{ mol}^{-1}$ for Buerger and Watanabe mechanisms respectively.

In view of the experimental observations of hysteresis in the applied pressure, we have calculated \bar{G} surfaces at applied pressures both higher than and lower than P_{trans} . The activation energies for B1 \rightarrow B2 and B2 \rightarrow B1 are different at all pressures except P_{trans} . At room temperature thermal contributions to the free energy are not large enough to overcome the energy barrier at P_{trans} . Pressures with thermally accessible barriers for the B1 \rightarrow B2 transition are larger than the thermodynamic transition pressures. For B2 \rightarrow B1, pressures with accessible barriers are smaller than P_{trans} .

Ref. 85 presents activation energies for a wider range of compounds calculated for the Buerger and WTM mechanisms using two-body potentials and discusses periodic trends. This area is clearly ripe for further investigation and a particularly interesting challenge will be the use of calculated activation energies and volumes together with nucleation theory to estimate the rates of solid state reactions more widely.

Transition metal oxides at high pressure

Our final example is the behaviour of MnO and NiO at high pressure. HF theory has been shown to give an accurate description of the zero-pressure ground-state electronic and magnetic structures of these compounds.^{7,87} Close agreement has been obtained between HF and experimental B1–B2 transition pressures for a wide range of alkali halides,^{85,88,89} alkaline-earth oxides,^{11,85} and the rutile to fluorite transition.^{39,90} It is of obvious interest to extend our studies of MnO and NiO to high pressure in order to address a number of unresolved issues for both compounds, which in several ways appear to behave unlike their isostructural s-block counterparts.

Shock wave experiments on MnO reported by Noguchi *et al.*⁹¹ indicate a pressure-induced phase transition from the NaCl-(B1) phase at $\approx 90 \text{ GPa}$. However, it is not clear whether this transition is simply to the CsCl-(B2) structure by analogy with CaO⁹² and SrO,⁸⁶ distorted CsCl as possibly in BaO,⁹³ or NiAs as in FeO,⁹⁴ and whether the new phase is metallic as with FeO⁹⁵ and NiO.⁹⁶ There appears to be no evidence of metallisation of the NaCl-phase up to 50 GPa .⁹⁷ To address these issues, calculations have been carried out⁹⁸ using the spin-unrestricted UHF procedure⁹⁹ to describe open-shell electronic configurations, and the same extended Gaussian basis sets for the different phases as in previous work.⁷

Optimised undistorted structural parameters at zero pressure and corresponding total energies for MnO in the NaCl, CsCl, zinc blende, wurtzite and NiAs structures were obtained⁹⁸ by direct minimisation of the Hartree–Fock energy. It is possible to calculate the lowest energy spin arrangements of each of these phases. For example, MnO is antiferromagnetic with the AF_2 spin arrangement in which the individual atomic moments are aligned in ferromagnetic (111) sheets, and adjacent sheets have antiparallel spin—but such calculations involve the use of larger unit cells and so are computationally more expensive. Previous studies^{7,100} indicate that the energy differences between the magnetic states and distortions associated with spin–lattice interactions are small compared with energy differences between different phases, and so it is unlikely that energy comparisons, based on the ferromagnetic ordering could lead to an incorrect order of stability. Energies and volumes at zero pressure for the five possible structures considered here, all of which were found to be insulating, are listed in Table 1. The NaCl structure is the predicted low temperature/low pressure phase, as observed. To a first approximation, the transition pressure between the B1 and B2 phases can be estimated from zero pressure data as $P_t \approx -(\Delta E/\Delta V)_{P=0}$. The volumes show that, of these five structures, the CsCl structure is the only possibility for the high-pressure phase, with $P_t \approx 140 \text{ GPa}$.

Equations of state and free energies in the static limit were calculated as for SrO in the previous section. Calculations using interatomic potentials and QLD indicate that at 300 K the change in transition pressure due to the inclusion of vibrational effects is negligible.^{85,101} Turning to consider the actual

Table 1 Hartree–Fock optimised structures and corresponding energies for MnO

Structure	$\Delta E_{\text{HF}}/\text{eV}$	$a/\text{\AA}$	$c/\text{\AA}$	$V/\text{\AA}^3$
NaCl	0.0	4.524 ^a	—	23.149
Wurtzite	0.13	3.477	5.550	29.058
Zinc blende	0.21	4.877	—	29.003
NiAs	0.38	3.140	5.520	23.570
CsCl	1.59	2.774	—	21.349

^a The experimental value of a is $4.445 \pm 0.001 \text{ \AA}$.

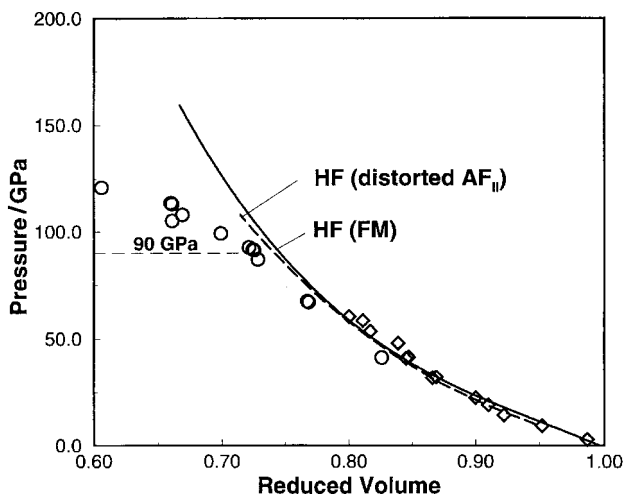


Fig. 14 Calculated and experimental Hugoniots for MnO. (○) experimental data from ref. 91, (◇) data from ref. 102.

high pressure structures, the NaCl-phase is high-spin insulating in both the FM and AF₂ spin arrangements up to a pressure of 210 GPa. Fig. 14 shows the full HF Hugoniot for the NaCl structure compared with the diamond-anvil data¹⁰² and the reduced shock compression results.⁹¹ The evident agreement between calculated and static compression data is strong evidence that MnO stays in the B1 phase, at least up to the limit of the static compression (≈ 60 GPa).

The CsCl structure is high-spin insulating up to 120 GPa, above which the UHF solutions are conducting. Since HF theory in the form used here gives an inadequate description of conducting phases, the properties of the metallic B2 phase were not considered further. As shown in Fig. 15, even at 120 GPa the NaCl-structure is still lower in free energy, so that a transition from insulating undistorted NaCl to undistorted insulating CsCl is not predicted by the UHF calculations. A value around 160 GPa for the hypothetical transition pressure is obtained by extrapolating the G vs. P plots of Fig. 15. This value is close to that obtained by extrapolation of a plot of transition pressure vs. cation radius for the alkaline-earth oxides.⁹⁸

Spin-lattice interaction in the AF₂ spin arrangement of the NaCl-phase leads to a small rhombohedral distortion of the lattice,¹⁰³ which earlier UHF calculations have predicted correctly.⁷ This rhombohedral distortion increases with pressure, lowering the energy of the NaCl-phase at all pressures con-

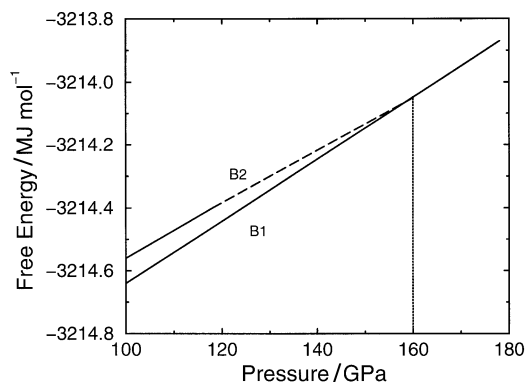


Fig. 15 Calculated free energies, in the static limit, as a function of pressure for the B1 and B2 phases of MnO. The dotted line denotes the extrapolation of the cubic B2 results, as described in the text.

sidered.⁹⁸ It leads to a small increase in the stability of the B1 phase at these pressures and so cannot account for the observed phase transition as involving insulating NaCl- and CsCl-phases.

In summary, MnO remains insulating with the NaCl structure up to the reported transition pressure of ≈ 90 GPa; this observed transition is incompatible with a non-metallisation transition to an undistorted CsCl-phase, but compatible with either a transition to a distorted CsCl-phase or a metallisation transition to a CsCl-phase. Explicit inclusion of *a posteriori* correlation corrections to the total Hartree-Fock energy based on the Perdew functional¹⁴ leaves these conclusions unchanged.⁹⁸

As with MnO, spin-lattice interaction in the AF₂ arrangement of NiO leads to a small rhombohedral distortion,¹⁰⁴ Sasaki has reported a density-functional study¹⁰⁵ of the rhombohedral distortion of the B1 phase of NiO at high pressure, and finds a much larger distortion at pressures above 60 GPa, predicting a hexagonal c/a ratio as low as ≈ 2.18 at 100 GPa. The magnitude of this distortion is such that we have found it worthwhile to extend our earlier zero-pressure studies⁷ in order to compare Sasaki's results with those from periodic unrestricted HF theory. Calculated and experimental^{106,107} Hugoniots are in good agreement as is clear from Fig. 16, and this has encouraged us to investigate possible rhombohedral distortions in the AF₂ arrangement in more detail. The results for this distortion as a function of pressure are shown in Fig. 17. We predict only a small decrease in the hexagonal c/a ratio with pressure, corresponding to an increase in the rhombohedral angle from $\sim 60.08^\circ$ at zero pressure to $\sim 60.18^\circ$ at 100 GPa. In marked contrast to

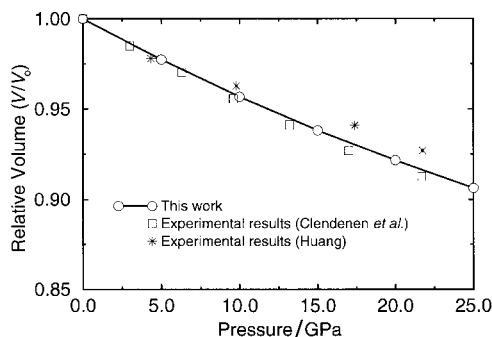


Fig. 16 Calculated and experimental Hugoniots for NiO (*) Denotes experimental data points from ref. 106. (□) experimental data from ref. 107.

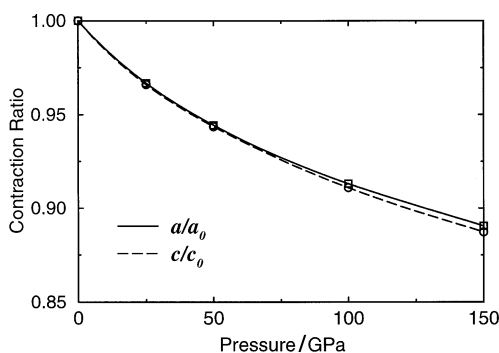


Fig. 17 Calculated variation with pressure of a/a_0 and c/c_0 (expressed in the hexagonal system) for NiO.

the DFT study of Sasaki,¹⁰⁵ we find no evidence of a change in behaviour with pressure associated with a sharp decrease in the c/a ratio at 60 GPa. It is clear from this discrepancy between HF and DFT that further work, both theoretical and experimental,¹⁰⁸ is essential to resolve this issue. These results for NiO also serve to illustrate the important point that high pressures, which can sample internuclear separations very different from those adopted under ambient conditions, serve as a stringent test of any theoretical method.

Final remarks

We have outlined, with the aid of a wide-ranging set of examples, how *ab initio*, QLD, MC and MD techniques, employed together in a powerful combination, provide valuable insight into the behaviour of perfect and defective polar solids at elevated temperatures and/or high pressures. Properties examined include thermal expansion coefficients, the isothermal Anderson–Grüneisen function, free energies of defect and surface formation, excess quantities of mixing and thermodynamic and mechanistic aspects of phase transitions. We have been able to assess critically common approximations used for many years, and have even made some predictions. Calculations at finite temperatures and/or high pressures are a sensitive test of any theoretical method, in large part due to the need to represent accurately the ionic interactions over a range of interatomic distances that may be far from those adopted at $T = 0$ and zero pressure.

Increasingly attention is moving from bulk properties to defect and surface properties at finite temperature and to solid solutions. In particular, new methods, such as HMC or explicit free energy minimisation of a large number of configurations, that are capable of dealing with high defect levels will increase considerably the contact between experiment and theory in many areas of materials and solid-state research. Although QLD usually fails above two-thirds of the melting point, it is an attractive strategy for the rapid evaluation of the free energy below this temperature and remains valid at low temperatures at which classical MC and MD fail. There is much scope for future applications ranging from the calculation of important ceramic and mineralogical data such as phase diagrams to new methods for kinetic and mechanistic aspects of solid state reactions. For example, our knowledge of the accretion and subsequent chemical differentiation of the Earth derives largely from chemical analyses of trace elements and their isotopes in rocks, and modelling and interpretation of these data require a detailed understanding of how trace elements are partitioned between coexisting phases,¹⁰⁹ often at high T and P .

Many of the dynamic properties examined here can be highly sensitive to the interionic potentials employed. Increasingly, too, attention is being paid to situations involving mechanisms and phase transitions where the energy differences involved may be very small indeed and highly potential dependent. Despite substantial developments in recent years in obtaining potentials directly from *ab initio* calculations, improved representations of the interionic interactions are urgently required. In the long run, as computer power continues to increase, it may well prove preferable to develop directly *ab initio* molecular dynamics and *ab initio* lattice dynamics techniques.

Acknowledgements

This work was supported by EPSRC and NERC. GDB acknowledges support from el Consejo Nacional de Investigaciones Científicas y Técnicas de la República Argentina and his contribution to this work has been possible due to a grant from the Fundación Antorchas. CES acknowledges support

from EPSRC and ICI. Help over a long period from Bill Mackrodt, Hugh Barron, Julian Gale, and Lev Kantorovich is gratefully acknowledged.

References

- 1 For example, *Computer Modelling in Inorganic Crystallography*, ed. C. R. A. Catlow, Academic Press, San Diego–London, 1997.
- 2 For example, C. Pisani, R. Dovesi and C. Roetti, *Hartree–Fock Ab Initio Treatment of Crystalline Systems*, Lecture Notes in Chemistry, Springer-Verlag, Berlin, 1988, vol. 48.
- 3 For example, B. Smit and D. Frenkel, *Understanding Molecular Simulation, From Algorithms to Application*. Academic Press, San Diego–London, 1996.
- 4 For example, M. T. Dove, *Introduction to Lattice Dynamics*, Cambridge University Press, Cambridge, 1993.
- 5 R. M. Fracchia, G. D. Barrera, N. L. Allan, T. H. K. Barron and W. C. Mackrodt, *J. Phys. Chem. Solids*, 1998, **59**, 435.
- 6 R. Dovesi, V. R. Saunders, C. Roetti, M. Causà, N. M. Harrison, R. Orlando and E. Aprà, *CRYSTAL 95, User Manual*, University of Turin and CCLRC Daresbury Laboratory, 1996.
- 7 M. D. Towler, N. L. Allan, N. M. Harrison, V. R. Saunders, W. C. Mackrodt and E. Aprà, *Phys. Rev. B*, 1994, **50**, 5041.
- 8 A detailed account of the effect of these tolerances has been given by R. Dovesi, M. Causà, R. Orlando, C. Roetti and V. R. Saunders, *J. Chem. Phys.*, 1990, **92**, 7402.
- 9 H. J. Monkhorst and J. D. Pack, *Phys. Rev. B*, 1976, **13**, 5188.
- 10 P. J. Hay and W. R. Wadt, *J. Chem. Phys.*, 1985, **82**, 270.
- 11 A. Zupan, I. Petek, M. Causà and R. Dovesi, *Phys. Rev. B*, 1993, **48**, 799.
- 12 S. H. Vosko, L. Wilk and M. Nusair, *Can. J. Phys.*, 1980, **58**, 1200.
- 13 For examples, see M. Causà and A. Zupan, *Chem. Phys. Lett.*, 1994, **220**, 145; M. Causà and A. Zupan, *Int. J. Quantum Chem.*, S, 1995, **28**, 633.
- 14 J. P. Perdew, J. A. Chevary, S. H. Vosko, K. A. Jackson, M. R. Pederson, D. J. Singh and C. Fiolhais, *Phys. Rev. B*, 1992, **46**, 6671.
- 15 M. B. Taylor, G. D. Barrera, N. L. Allan, T. H. K. Barron and W. C. Mackrodt, *Comput. Phys. Commun.*, 1998, **109**, 135.
- 16 For example, D. Fincham, W. C. Mackrodt and P. J. Mitchell, *J. Phys. Condens. Matter*, 1994, **6**, 393.
- 17 For example, J. D. Gale, *J. Phys. Chem. B*, 1998, **102**, 5423 and references therein.
- 18 N. L. Allan, T. H. K. Barron and J. A. O. Bruno, *J. Chem. Phys.*, 1996, **105**, 8300.
- 19 B. G. Dick and A. W. Overhauser, *Phys. Rev.*, 1958, **112**, 90.
- 20 A. A. Maradudin, *The Theory of Lattice Dynamics in the Harmonic Approximation*, Solid State Physics, vol. 3, Academic Press, New York, 1971.
- 21 For a full discussion of static lattice simulations see C. R. A. Catlow and W. C. Mackrodt, in *Computer Simulation of Solids*, ed. C. R. A. Catlow and W. C. Mackrodt, Springer-Verlag, Berlin, 1982, ch. 1.
- 22 For example, D. C. Wallace, *Thermodynamics of Crystals*, Wiley, New York, 1972.
- 23 For example, D. J. Chadi and M. L. Cohen, *Phys. Rev. B*, 1973, **8**, 5747.
- 24 T. H. K. Barron, T. G. Gibbons and R. W. Munn, *J. Phys. C: Solid State Phys.*, 1971, **4**, 2805.
- 25 T. G. Gibbons, *Phys. Rev. B*, 1973, **7**, 1410.
- 26 A. B. Pippard, *The Elements of Classical Thermodynamics*, Cambridge University Press, Cambridge, 1964.
- 27 M. B. Taylor, G. D. Barrera, N. L. Allan and T. H. K. Barron, *Phys. Rev. B*, 1997, **57**, 14380.
- 28 M. B. Taylor, N. L. Allan, J. A. O. Bruno and G. D. Barrera, *Phys. Rev. B*, 1999, **59**, 353.
- 29 M. B. Taylor, C. E. Sims, G. D. Barrera and N. L. Allan, *Phys. Rev. B*, 1999, **59**, 6742.
- 30 P. J. Harley, in *Numerical Algorithms*, ed. J. L. Mohamed and J. E. Walsh, Clarendon Press, Oxford, 1986, p. 239.
- 31 W. H. Press, S. A. Teukolsky, W. T. Vetterling and B. P. Flannery, *Numerical Recipes in Fortran*, Cambridge University Press, Cambridge–New-York–Victoria, 2nd edn. 1992, p. 420.
- 32 M. P. Allen and D. J. Tildesley, *Computer Simulation of Liquids*, Clarendon Press, Oxford, 1987.
- 33 S. Melchionna, G. Ciccotti and B. L. Hulan, *Mol. Phys.*, 1993, **78**, 533.
- 34 J. A. Purton, G. D. Barrera, N. L. Allan and J. D. Blundy, *J. Phys. Chem. B*, 1998, **102**, 5202.

- 35 For example, M. E. Clamp, P. G. Baker, C. J. Stirling and A. Brass, *J. Comput. Chem.*, 1994, **15**, 838.
- 36 Q. Wang, J. K. Johnson and J. Q. Broughton, *Mol. Phys.*, 1996, **89**, 1105.
- 37 J. A. Purton, J. D. Blundy, M. B. Taylor, G. D. Barrera and N. L. Allan, *Chem. Commun.*, 1998, 627.
- 38 For example, K. D. Heath, W. C. Mackrodt, V. R. Saunders and M. Causà, *J. Mater. Chem.*, 1994, **4**, 825.
- 39 G. D. Barrera, M. B. Taylor, N. L. Allan, T. H. K. Barron, L. N. Kantorovich and W. C. Mackrodt, *J. Chem. Phys.*, 1997, **107**, 4337.
- 40 *Thermophysical Properties of Matter* (TPRC Data Series), ed. Y. S. Touloukian, R. K. Kirby, R. E. Taylor and T. Y. R. Lee, IFI/Plenum, New York–Washington, 1977, vol. 13.
- 41 D. L. Anderson, *Phys. Earth Planet Int.*, 1987, **45**, 307.
- 42 N. L. Allan, M. Braithwaite, D. L. Cooper, W. C. Mackrodt and S. C. Wright, *J. Chem. Phys.*, 1991, **95**, 6792.
- 43 A. Chopelas, *Phys. Chem. Miner.*, 1990, **17**, 142.
- 44 A. Chopelas and R. Boehler, *Geophys. Res. Lett.*, 1989, **16**, 1347.
- 45 T. A. Mary, J. S. O. Evans, T. Vogt and A. W. Sleight, *Science*, 1996, **272**, 90.
- 46 J. S. O. Evans, T. A. Mary, T. Vogt, M. A. Subramanian and A. W. Sleight, *Chem. Mater.*, 1996, **8**, 2809.
- 47 T. H. K. Barron, *Thermal Expansion of Solids*, vol. I-4 in the CINDAS Data Series on Material Properties, ed. C. Y. Ho, ASM International, Materials Park, OH, 1998, ch. 1, pp. 1–104.
- 48 A. K. A. Pryde, K. D. Hammonds, M. T. Dove, V. Heine, J. D. Gale and M. C. Warren, *J. Phys. Condens. Matter*, 1996, **8**, 10973. The interionic potentials used by these authors lead to imaginary frequencies at certain q -vectors so rendering their potential model invalid.
- 49 N. L. Allan, G. D. Barrera, J. A. O. Bruno and T. H. K. Barron, in preparation.
- 50 J. S. O. Evans, Z. Hu, J. D. Jorgensen, D. N. Argyriou, S. Short and A. W. Sleight, *Science*, 1997, **275**, 61.
- 51 P. Tschaufeser and S. C. Parker, *J. Phys. Chem.*, 1995, **99**, 10609.
- 52 J. W. Couves, R. H. Jones, S. C. Parker, P. Tschaufeser and C. R. A. Catlow, *J. Phys. Condens. Matter*, 1993, **5**, 329.
- 53 P. W. Tasker, in *Computer Simulation of Solids*, ed. C. R. A. Catlow and W. C. Mackrodt, Springer-Verlag, Berlin, 1982, p. 288.
- 54 For example, W. C. Mackrodt, *Adv. Ceram.*, 1987, **23**, 293; W. C. Mackrodt, R. J. Davey, S. N. Black and R. Docherty, *J. Cryst. Growth*, 1987, **80**, 441; N. L. Allan, A. L. Rohl, D. H. Gay, C. R. A. Catlow, R. J. Davey and W. C. Mackrodt, *Faraday Discuss.*, 1993, **95**, 273; R. I. Hines, N. L. Allan and W. R. Flavell, *J. Chem. Soc., Faraday Trans.*, 1996, **92**, 2057.
- 55 D. H. Gay and A. L. Rohl, *J. Chem. Soc., Faraday Trans.*, 1995, **91**, 925 and references therein.
- 56 D. M. Heyes, M. Barber and J. H. R. Clarke, *J. Chem. Soc., Faraday Trans. 2*, 1977, **10**, 1485.
- 57 P. M. Oliver, G. W. Watson and S. C. Parker, *Phys. Rev. B*, 1995, **52**, 5323.
- 58 (a) P. A. Mulheran and J. H. Harding, *Ceram. Trans.*, 1992, **24**, 3; (b) P. A. Mulheran and J. H. Harding, *J. Phys. IV*, 1993, **3**, 1971.
- 59 P. A. Mulheran, *Philos. Mag. A*, 1993, **68**, 799.
- 60 A. M. Stoneham and M. J. L. Sangster, *Philos. Mag. B*, 1981, **43**, 597.
- 61 G. C. Benson and K. S. Yun, *The Solid–Gas Interface*, ed. E. A. Flood, Arnold, London, 1967.
- 62 K. H. Rieder, *Surf. Sci.*, 1971, **26**, 637.
- 63 T. S. Chen and F. W. de Wette, *Surf. Sci.*, 1978, **74**, 373.
- 64 C. E. Sims, PhD Thesis, University of Bristol, 1999.
- 65 M. B. Taylor, G. D. Barrera, N. L. Allan, T. H. K. Barron and W. C. Mackrodt, *Farad. Discuss.*, 1997, **106**, 377.
- 66 C. R. A. Catlow, J. Corish, P. W. M. Jacobs and A. B. Lidiard, *J. Phys. C: Solid State Phys.*, 1981, **14**, L125.
- 67 N. L. Allan, W. C. Mackrodt and M. Leslie, *Adv. Ceram.*, 1987, **23**, 257.
- 68 G. V. Lewis and C. R. A. Catlow, *J. Phys. C: Solid State Phys.*, 1985, **18**, 1149.
- 69 R. D. Shannon, *Acta Crystallogr., Sect. A*, 1976, **32**, 751.
- 70 H. Gripenberg, S. Seetharaman and L. I. Staffansson, *Chem. Scr.*, 1978–79, **13**, 162.
- 71 S. Raghavan, PhD Thesis, Indian Institute of Science, Bangalore, 1971.
- 72 For example, B. J. Wood, R. T. Hackler and D. P. Dobson, *Contrib. Miner. Petrol.*, 1994, **115**, 735.
- 73 J. A. Purton, N. L. Allan and J. D. Blundy, *Chem. Commun.*, 1999, 707.
- 74 M. Matsui and G. D. Price, *Nature*, 1991, **351**, 735.
- 75 The experimental evidence is contradictory—*e.g.*, E. Knittle and R. Jeanloz, *Science*, 1987, **235**, 668; C. Meade, H. K. Mao and J. Hu, *Science*, 1995, **268**, 1743.
- 76 N. L. Allan, M. Braithwaite, D. L. Cooper, W. C. Mackrodt and B. Petch, *J. Chem. Soc., Faraday Trans.*, 1993, **89**, 4369 and references therein; C. E. Sims, N. L. Allan and T. H. K. Barron, *Phys. Rev. B*, 1999, **60**, 2968.
- 77 N. L. Allan, M. Braithwaite, D. L. Cooper, W. C. Mackrodt and B. Petch, *Mol. Simul.*, 1992, **9**, 161.
- 78 For example, O. Blaschko, G. Ernst, G. Quittner, G. Pépy and M. Roth, *Phys. Rev. B*, 1987, **36**, 474.
- 79 M. Watanabe, M. Tokonami and N. Morimoto, *Acta Crystallogr., Sect. A*, 1977, **33**, 294.
- 80 For example, A. R. West, *Solid State Chemistry and its Applications*, Wiley, New York, 1984.
- 81 H. Shoji, *Z. Kristallogr.*, 1931, **77**, 381.
- 82 J. Buerger, in *Phase Transformation in Solids*, ed. R. Smoluchowski, J. E. Mayers and W. A. Weyl, Wiley, New York, 1951.
- 83 For an animation, see <http://www.rsc.org/suppdata/cp/a9/a908622f>.
- 84 M. Gufan and I. V. Ternovskii, *Phys. Solid State*, 1993, **35**, 639.
- 85 C. E. Sims, G. D. Barrera, N. L. Allan and W. C. Mackrodt, *Phys. Rev. B*, 1998, **57**, 11164.
- 86 Y. Sato and R. Jeanloz, *J. Geophys. Res.*, 1981, **86**, 1773.
- 87 W. C. Mackrodt, N. M. Harrison, V. R. Saunders, N. L. Allan, M. D. Towler, E. Aprà and R. Dovesi, *Phil. Mag. A*, 1993, **68**, 653.
- 88 E. Aprà, M. Causà, M. Prencipe, R. Dovesi and V. R. Saunders, *J. Phys. Condens. Matter*, 1993, **5**, 2969.
- 89 R. L. Erikson, E. Eary and C. J. Hostetler, *J. Chem. Phys.*, 1993, **99**, 336.
- 90 N. L. Allan, R. I. Hines, M. D. Towler and W. C. Mackrodt, *J. Chem. Phys.*, 1994, **100**, 4710.
- 91 Y. Noguchi, K. Kusaba, K. Fukuoka and Y. Syono, *Geophys. Res. Lett.*, 1996, **23**, 1469.
- 92 P. Richet, H. K. Mao and P. M. Bell, *J. Geophys. Res.*, 1988, **93**, 15297.
- 93 L. Liu and W. A. Bassett, *J. Geophys. Res.*, 1972, **77**, 4934.
- 94 Y. Fei and H. K. Mao, *Science*, 1994, **266**, 1678.
- 95 E. Knittle, R. Jeanloz, A. C. Mitchell and W. J. Nellis, *Solid State Commun.*, 1986, **59**, 513.
- 96 N. Kawai and S. Mochizuki, *Solid State Commun.*, 1971, **9**, 1393.
- 97 Y. Syono, T. Goto, J. Nakai and Y. Nakagawa, *Rev. Phys. Chem. Jpn.*, 1975, 466.
- 98 W. C. Mackrodt, E.-A. Williamson, D. Williams and N. L. Allan, *Phil. Mag. B*, 1998, **77**, 1063.
- 99 J. A. Pople and R. K. Nesbet, *J. Chem. Phys.*, 1954, **22**, 571.
- 100 R. I. Hines, N. L. Allan, G. S. Bell and W. C. Mackrodt, *J. Phys. Condens. Matter*, 1997, **9**, 7105.
- 101 We find that the thermal pressure is only a very weak function of the volume. This is one of the assumptions of the so-called “Universal Equations of State”, *e.g.*, P. Vinet, J. R. Smith, J. Ferrant and J. H. Rose, *Phys. Rev. B*, 1987, **35**, 1945.
- 102 R. Jeanloz and A. Ruddy, *J. Geophys. Res.*, 1987, **92**, 11455.
- 103 H. Shaked, J. Faber and R. L. Hittermann, *Phys. Rev. B*, 1988, **38**, 11901.
- 104 G. A. Slack, *J. Appl. Phys.*, 1960, **31**, 1571.
- 105 T. Sasaki, *Phys. Rev. B*, 1996, **54**, R9581.
- 106 E. Huang, *High Pressure Res.*, 1995, **13**, 307.
- 107 R. L. Clendenen and H. G. Drickamer, *J. Chem. Phys.*, 1966, **44**, 4223.
- 108 D. R. Allan, W. C. Mackrodt and N. L. Allan, in preparation.
- 109 For example, J. A. Purton, N. L. Allan, J. D. Blundy and E. A. Wasserman, *Geochim. Cosmochim. Acta*, 1996, **60**, 4977.